Journal of Electroceramics, 10, 165–177, 2003

A Strategy for Analysis and Modelling of Impedance Spectroscopy Data of Electroceramics: Doped Lanthanum Gallate

E.J. ABRAM, D.C. SINCLAIR & A.R. WEST*

Department of Engineering Materials, Sir Robert Hadfield Building, University of Sheffield, Mappin Street, Sheffield, S1 3JD, UK

Submitted March 11, 2003; Revised August 1, 2003; Accepted October 13, 2003

Abstract. Modelling of impedance spectroscopy (IS) data of electroceramics depends critically on the correct choice of equivalent electrical circuit so that the extracted parameters have physical significance. The strategy proposed to choose the correct circuit involves analysis of IS data in several of the four complex formalisms: impedance, electric modulus, admittance and permittivity together with consideration of the frequency and temperature dependence of data and the magnitude and temperature dependence of extracted resistance and capacitance values. This is demonstrated using IS data from oxide-ion conducting $La_{0.80}Sr_{0.20}Ga_{0.83}Mg_{0.17}O_{2.82}$ ceramics over the range 182 to 280°C. Low temperature data are fitted first, to allow a full characterisation of the bulk response; some of the bulk parameters may then be fixed to enable fitting of the higher temperature data which increasingly feature lower frequency phenomena such as grain boundary impedances. The most appropriate circuit in this case is found to consist of a parallel combination of a resistor, capacitor and constant phase element (CPE) for the bulk response in series with a resistor and capacitor in parallel for a constriction resistance. The origin of the constriction resistance may be associated with the presence of plate-like $LaSrGaO_4$ secondary phase within the grains and/or with the presence of pores at the grain boundaries. The importance of choosing (a) the correct equivalent circuit and (b) approximately correct input values for the various circuit parameters to be fitted and refined are demonstrated.

Keywords: impedance spectroscopy, equivalent circuit analysis, oxide-ion conductors

1. Introduction

Impedance spectroscopy (IS) is an extremely useful technique to analyse the electrical properties of a wide variety of electroceramics, including ferroelectrics, solid electrolytes and mixed conductors. In many cases, ceramics contain both intra- and intergranular impedances connected in series and IS can be used to establish the temperature dependence of the resistive, R, and capacitive, C, components of each region. To extract this information, it is essential to model experimental data using an equivalent electrical circuit, i.e. some combination of resistors, capacitors and constant phase elements (CPEs) connected in series and/or parallel, that gives the same impedance response as the ceramic. A link is then made between features in the sample and elements in the equivalent circuit; this is aided by consideration of the magnitude of the different R and C components and their temperature dependence.

Two approaches are commonly employed in analysis of IS data. The first is to assume an equivalent circuit based on visual inspection of the data, normally impedance (Z^*) complex plane (Z'' vs. Z') plots, and to extract the various R and C values by a simple hand-fitting procedure. The second, more quantitative approach is to model the data using various equivalent circuits and, depending on the quality of agreement between experimental and simulated data, chose the most appropriate circuit to extract R and C values. The major difficulty over the interpretation of IS data, however, is that it is usually possible to fit a number of plausible equivalent circuits to a given data set; clearly

*To whom all correspondence should be addressed. E-mail: a.r.west@sheffield.ac.uk

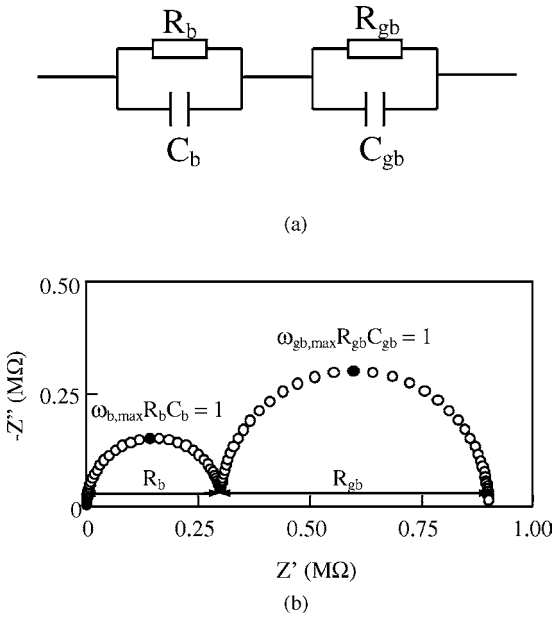

Fig. 1. (a) An equivalent electrical circuit commonly used to model IS data of electroceramics, and (b) a Z^* plot for $R_b = 0.3$ MΩ, $C_b = 5$ pF, $R_{gb} = 0.6$ MΩ, $C_b = 1$ nF.

a critical assessment is required to decide which circuit is most appropriate, but there are few well-established guidelines to aid this assessment.

In many electroceramics, the resistance of grain boundaries exceeds that of the grains and restricts the flow of current. Figure 1(a) shows a circuit commonly assumed to model such ceramics and Fig. 1(b) shows a typical Z^* plot for such a circuit which consists of two semi-circular arcs. R_b and R_{gb} correspond to the resistance of the bulk and grain boundary regions, respectively, and can be estimated as shown. The bulk and grain boundary capacitances, C_b and C_{gb}, respectively, can be estimated using the relationship $\omega_{max}RC = 1$, where $\omega_{max} = 2\pi f_{max}$ and f_{max} is the applied frequency at each arc maximum. Assignment of arcs to the bulk and grain boundary regions is based on the magnitude of the associated capacitance, assuming a brick-work model for the ceramic microstructure. In many [1] cases, the lower frequency (grain boundary) arc has an associated capacitance in the nF range and the higher frequency (bulk) arc has an associated capacitance of a few pF. The resolution of arcs depends on the difference between their associated time constants, τ, where $\tau = RC$ for each parallel RC element. Generally, differences between time constants of greater than two orders of magnitude give well-resolved arcs.

The circuit in Fig. 1(a) shows no impedance contribution associated with the sample-electrode interface. In practice, an additional impedance is often present, associated with either (partially) blocking phenomena if the conducting species in the ceramic are ions or with contact impedances associated with Fermi level differences between ceramic and electrode if the conducting species are electrons. In this paper, we are excluding from consideration such electrode/sample impedance phenomena; they are usually readily recognisable in most oxide ion conductors since they have capacitances of about 10^{-7} F or higher, typical of double layer effects.

In practice, most samples do not exhibit the ideal 'Debye-like' behaviour shown in Fig. 1(b); instead, arcs are depressed with their centres displaced below the real axis. Such deviations from ideal behaviour are often ignored when hand-fitting data and computer-based curve fitting is time-consuming. Nevertheless, modelling non-ideal responses and establishing the most appropriate equivalent circuit to represent the electrical properties is an absolutely essential step towards a correct understanding of electroceramics, especially those that are chemically doped to create electrically heterogeneous regions within the ceramic. In such cases, curve fitting and the testing of various equivalent circuits is essential.

In order to model non-ideal IS data, CPEs are usually used in addition to resistors and capacitors. A CPE has an impedance (Z^*_{CPE}) defined as

$$Z^*_{CPE} = [\mathbb{A}(j\omega)^n]^{-1} \tag{1}$$

where A ($\mathbb{A} = A/\cos(n\pi/2)$ where A is a constant that has been used in previous studies [2]) and n are constants and $j = \sqrt{-1}$. Non-ideal Debye-like behaviour of many electroceramics and especially, the bulk component of ionic conductors is well-documented and can often be successfully modelled using a parallel combination of R, C and CPE components (Fig. 2). The best method of fitting this circuit to the bulk data is to examine spectroscopic plots of the real part of the complex admittance, Y^*. The expression for Y' for the circuit shown is:

$$Y' = R^{-1} + \mathbb{A}\omega^n \cos(n\pi/2) \tag{2}$$

In a spectroscopic plot of log Y' against log ω, a frequency-independent plateau at low frequencies, where $Y' \approx R^{-1}$, is followed by a 'cross-over'

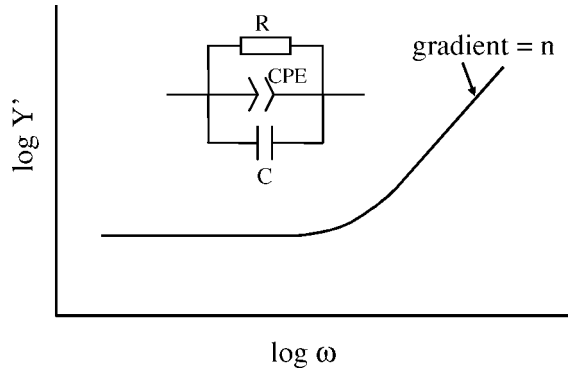

Fig. 2. Schematic plot of log Y' against log ω illustrating a low frequency plateau and a high frequency dispersion for an electroceramic, and a possible equivalent electrical circuit to model the behaviour.

region to a high frequency 'dispersion' where log Y' increases linearly with log ω (Fig. 2). The value of n gives the gradient of the linear dispersion region, and $\log[\mathrm{A}\cos(n\pi/2)]$ is the extrapolated intercept with the log Y' axis at $\omega = 1$ Hz. Non-ideal Debye-like behaviour of individual electro-active regions can be modelled by a variety of circuit elements and combinations, such as that shown in Fig. 2, or by replacing R or C in a parallel RC element (as in Fig. 1(a)) with a CPE.

A well-recognised problem with equivalent circuit analysis is that it may be difficult to select the correct equivalent circuit. One objective of this paper is to demonstrate a strategy that can be used to assist this process. As part of this strategy, it is necessary to test competing equivalent circuits to establish which gives the best fit to the data. It is essential to give full weighting to the IS data over the entire measured frequency spectrum and for this reason, care is required over data presentation to ensure that data over certain frequency ranges are not 'hidden'. Since values of the real and imaginary parts of the different formalisms can vary by several orders of magnitude over the measured frequency range, use of complex plane plots on a linear-linear scale highlight data of the largest magnitude, and can easily give rise to an over-simplified model, as can spectroscopic plots of Z'', M'' vs. log(frequency) if the Z'', M'' data are presented using linear scales, where M'' is the imaginary part of the electric modulus. As an alternative, log-log plots ensure equal weighting of data over the entire frequency range and allow a more critical assessment of data fitting; such plots are not yet in common usage, however. The strategy presented here has two components. First, data are presented on linear scales to get an initial, visual overview of the impedance response; it is particularly valuable to present data as combined Z'', M'' spectroscopic plots which highlight different features of the impedance response. Second, data are presented on logarithmic scales to allow accurate assessment of the quality of fit of various model circuits.

It can also be valuable to analyse data collected over a range of temperatures; since most electrical processes are thermally activated, each one will be observable over only a limited range of temperatures within the given window of available measuring frequencies. A more comprehensive overview of the electrical make-up of a material is therefore obtained if data can be obtained over a range of temperature; in addition, this can help discriminate between possible equivalent circuits.

Z^* plots are the most commonly-used presentation of IS data. In principle, all the information required to deduce an equivalent circuit is contained within Z^* plots, but it may not be readily accessible when these are plotted on linear scales. Instead, the same data may either be re-plotted on logarithmic scales or transformed to one of the other three impedance formalisms: admittance, Y^*, relative permittivity, ε^* and relative electric modulus, M^*, using the equations:

$$Y^* = 1/Z^* \tag{3}$$

$$\varepsilon^* = 1/M^* \tag{4}$$

$$M^* = j\omega C_\mathrm{o} Z^* \tag{5}$$

$$\varepsilon^* = Y^*/j\omega C_\mathrm{o} \tag{6}$$

where C_o is the vacuum capacitance of the sample holder and electrode arrangement. Since different weighting factors are inherent in the use of these formalisms, additional insight into the appropriate equivalent circuit may be gained. Specifically, the correct equivalent circuit must give a good fit to *all* four formalisms and not just to Z^* plots.

A good example to illustrate the dependence on frequency and weighting of the various impedance formalisms is the use of a combination of Z^* and M^* complex plane plots (or Z'' and M'' spectra) to analyse IS data of positive temperature coefficient of resistance (PTCR) $BaTiO_3$ thermistors that contain insulating grain boundaries and semi-conducting grains [3].

From Eq. (5),

$$M^* = M' + jM'' = j\omega C_o Z^* = j\omega C_o(Z' - jZ'')$$
$$= \omega C_o Z'' + j\omega C_o Z'.$$

Hence, $M' = \omega C_o Z''$ and $M'' = \omega C_o Z'$. Detailed consideration of the equations for M'' and Z'' shows that for a circuit consisting of a single parallel RC element, Z'' and M'' have the same functional form, giving rise to a Debye peak when plotted against frequency, but have different weighting factors in that the Z'' peak is scaled according to R whereas the M'' peak is scaled according to C^{-1}. Hence, Z^* and M^* complex plane plots (or Z'' and M'' spectra) highlight different aspects of the same data. Since Z^* plots are dominated by R_{gb} if $R_{gb} \gg R_b$, they provide useful information about the grain boundaries but little or no information on the bulk response. Any equivalent circuit analysis based only on conventional Z^* plots, therefore, does not necessarily provide adequate weighting to the bulk response of such ceramics. In contrast, M^* plots are dominated by the bulk response since $C_b \ll C_{gb}$ but provide little or no information about the grain boundaries. Thus, by using a combination of formalisms, different aspects of the same data are highlighted [3].

This brings us to the critical step in data interpretation and analysis. Often, no prior information about the expected equivalent circuit and/or magnitudes of resistance and/or capacitance for a sample is available. The approach that we adopt in such cases is to first, visually inspect the data in at least two of the four formalisms, usually Z^* and M^*, and determine the number of RC circuit combinations that are likely to be needed to model and fit the data. For most samples, a series combination of parallel RC elements is usually appropriate, which is why Z^* and M^* formalisms are used since each parallel RC element gives rise to its own Z'', M'' peaks. A range of equivalent circuits with, or without CPEs in addition to, or in place of the R and C components are then fitted to the data. The quality of the fits over the entire frequency range, for all four formalisms is assessed.

In the early stages of data analysis, especially if the equivalent circuits contain a large number of fitting parameters and all are allowed to vary simultaneously, it may be difficult to obtain a fully satisfactory fit. An important strategy is then to focus on a range of temperatures over which one particular feature of the impedance response is dominant. Our preference is to analyse first the lowest temperature data in which the bulk response of the sample is dominant and for which the circuit in Fig. 2 is usually appropriate. This region of the *ac* spectrum, when $\log Y'$ is plotted against $\log \omega$, should contain a low frequency plateau which may, or may not overlap with dispersions at lower frequencies associated with the onset of grain boundary or other thin layer phenomena, together with the high frequency dispersion characterised by a power law, with a gradient equal to n. Only at the lowest temperatures, is the power law dispersion adequately displayed since it is a high frequency effect that moves to increasingly higher frequencies with increasing temperature. In our experience, all ionic conductors and electronic semiconductors show this bulk power law dispersion, which is an example of Jonscher's 'Universal Law of Dielectric Response' [4] and therefore, to recognise and characterise this region of the *ac* spectrum provides a good starting point in data analysis. If suitable low temperature data are not available and instead, only the onset of the power law dispersion is seen, overlapping with the bulk conductivity plateau, then it is very easy to obtain erroneous values of n and A by fitting over a limited data set. In such cases, n may be fixed at a typical value of 0.6.

Once the data in the region of the bulk response have been fitted, higher temperature data may be considered by fixing, if necessary, the value for n of the bulk response (n usually shows little temperature dependence). It should then be possible, progressively, to find the best circuit to model the grain boundary and other, lower frequency components.

The temperature dependence of R and/or C values extracted from the data analysis using various equivalent circuits may also be useful in discriminating between circuits. Thermally-activated resistances associated with electronic and ionic conduction are commonly governed by the Arrhenius law. A plot of $\log(R^{-1})$ against reciprocal temperature should be linear unless curvature associated with phenomena such as extrinsic-intrinsic crossover, phase transitions, especially order-disorder transitions, and defect dissociation occurs. In the absence of such effects, any departure from linear, Arrhenius-type behaviour for R_b and R_{gb} and/or unexpected high or low activation energies may be evidence for an incorrect equivalent circuit. With the exception of ferroelectric materials, capacitance values usually have little or no temperature dependence. For ferroelectric materials in the temperature range above the Curie temperature, T_c, the capacitance

data should follow Curie-Weiss behaviour, with a linear dependence of C^{-1} on temperature, and this is a useful diagnostic. Anomalous values or temperature dependence of capacitance may indicate an incorrect equivalent circuit.

In our experience, when considering each of the points above, it is usually possible to find one equivalent circuit that accurately fits IS data over a wide ω, T range in all four formalisms and which gives a physically reasonable set of R, C values. In particular, it is often possible to discriminate between equivalent circuits which appear to give acceptable fits to Z^* plots. Here we illustrate this approach to analyse data for oxide-ion conducting $La_{0.80}Sr_{0.20}Ga_{0.83}Mg_{0.17}O_{2.82}$ ceramics over the temperature range ~182 to 280°C.

2. Experimental

$La_{0.80}Sr_{0.20}Ga_{0.83}Mg_{0.17}O_{2.82}$ (LSGM) ceramics were synthesised by a solid state route. Stoichiometric amounts of La_2O_3 (99.99% pure), Ga_2O_3 (99.995%), MgO (reagent grade) and $SrCO_3$ (99.9%+) powders were milled together in water with zirconia beads. The La_2O_3 and MgO powders were dried at 1000°C prior to weighing. After drying, the mixture was calcined at 1250°C for 6 hours, milled and dried. Pellets were pressed uniaxially at about 50 MPa and sintered at 1470°C for 6 hours. Phase purity was checked by X-ray diffraction (XRD) using a Guinier-Hägg camera with Cu Kα_1 radiation of wavelength 1.5405 Å, and by Scanning Electron Microscopy (SEM) using a JEOL JSM 6400 scanning electron microscope with a 20 kV accelerating voltage. Ceramic density as a percentage of the theoretical X-ray density was calculated using LSGM lattice parameters and the mass and dimensions of the ceramics.

Sputtered gold electrodes were deposited on ceramic samples for 8 minutes at 20 mA current under argon using an Emscope SC500 gold sputter-coater. Samples were connected to a measuring jig and placed in a non-inductively wound furnace where the temperature was controlled to ±2°C over the temperature range 150 to 300°C. IS was performed at ~10°C intervals using a Hewlett Packard 4192A impedance analyser at frequencies ranging from 5 Hz to ~13 MHz. IS data were corrected for the geometric factor of the sample (thickness/electrode area), the stray capacitance of the measuring jig and the resistance and inductance of the measuring leads. Corrected data were modelled with various equivalent electrical circuits using ZView equivalent circuit fitting software [5]. At frequencies above 1 MHz, the impedance data were unreliable due to inductive effects and were excluded.

3. Equivalent Circuit Analysis

IS data were analysed assuming a brickwork model for the ceramic microstructure; four equivalent circuits, A, B, C and D, shown in Fig. 3, were used to try and attain the best fit to the experimental data. Circuits A–C assume the ceramic response to be modelled on a bulk component only, whereas circuit D, assumes a series combination of two components which would represent bulk and grain boundary regions. The lower frequency limit for modelling the data was chosen from Z^* and/or ε' spectroscopic plots so as to exclude, as far as possible, data associated with the electrode processes (see Fig. 4). This was necessary as it was not possible to obtain sufficient data from the available

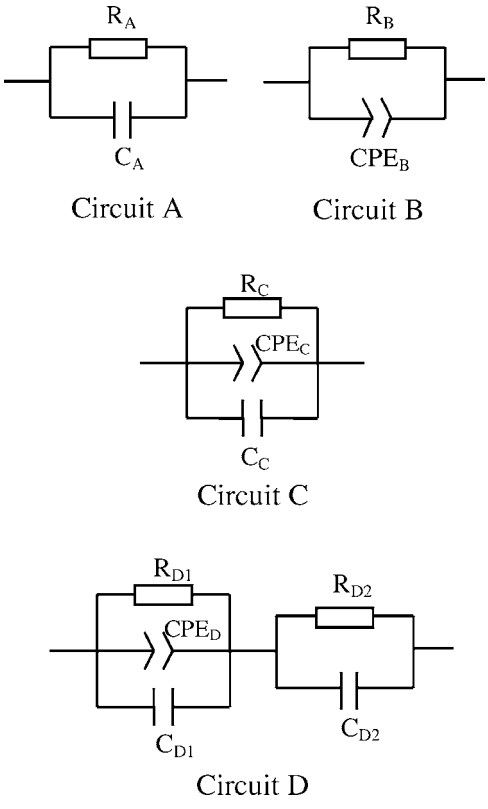

Fig. 3. Equivalent electrical circuits A, B, C and D used to model IS data from an LSGM ceramic.

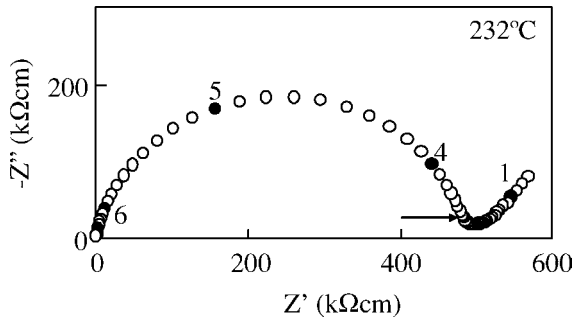

Fig. 4. Z^* plot of IS data from a LSGM ceramic obtained at 232°C. The arrow indicates the lower frequency limit for modelling the data. Selected frequencies (in Hz), on a logarithmic base 10 scale, are shown as filled circles.

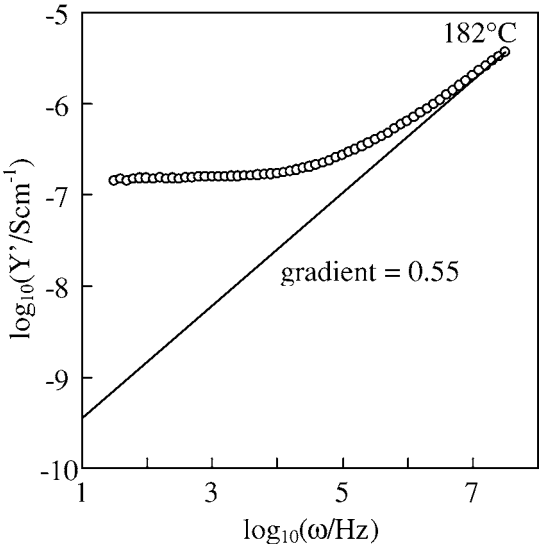

Fig. 5. log-log Y' spectroscopic plot of data obtained at 182°C. The estimated linear extrapolation of the dispersion region used to extract input values of n and A for the CPEs is shown.

frequency range to model *both* the ceramic *and* electrode interface responses at a given temperature. In this case, we chose to analyse data measured at ∼182 to 280°C, which allowed the ceramic response to be studied in detail. IS data were typically as shown in Fig. 4, with a broad, asymmetric, depressed arc and a lower frequency spike. In this work, we have analysed only the data corresponding to the arc. Circuit component values are quoted to two significant figures; the errors predicted by the fitting software were typically in the third significant figure.

As part of the fitting procedure it is necessary to input starting values for the various components of each circuit. As shown later, these values should be approximately correct; if not there is the possibility that they can refine into a false minimum.

Circuit A. Input values of R_A and C_A for each temperature were estimated by hand-fitting of data. R_A was estimated from the diameter of the arc in the Z^* plots, and C_A using the relationship $\omega_{max}RC = 1$ from the frequency at the top of the arc. The fitting software refined R_A and C_A to obtain the best fit to the data at each temperature.

Circuit B. Input values of n and A for CPE_B were estimated by hand-fitting of Y' data measured at 182°C as shown in Fig. 5, giving values of 0.55 and 4.8×10^{-10} S s^n, respectively. R_B was estimated in the same way as R_A. R_B, n and A were then freely refined to give the best fit to the data. For higher temperature data sets, n was fixed at the value obtained from the refinement at 182°C, 0.89; R_B and A were allowed to refine. n was fixed because the data associated with the linear dispersion region in log Y' spectroscopic plots became increasingly inaccessible above 182°C.

Circuit C. Modelling was performed in a similar way to circuit *B*. C_C was estimated in the same way as C_A. n was fixed at 0.64 to refine the higher temperature data.

Circuit D. A similar approach was used as for circuit *C* except that input values of R_{D1}, R_{D2} and C_{D2} could not be estimated accurately by hand-fitting. R_{D1} and R_{D2} were given starting values of 4/5 and 1/5 of the diameter of the arc in the Z^* plot, respectively, so making the assumption that the data are dominated by the parallel R-C-CPE element. C_{D2} was given a starting value of 10^{-10} F which is typical of a grain-boundary capacitance. All variables were allowed to freely refine for the 182°C data. For refinement of higher temperature data sets, n was fixed as before with a value of 0.59.

4. Results

The LSGM ceramics were found to be phase-pure by XRD but SEM showed the presence of two minor secondary phases. One was intra-granular and had a plate-like morphology and the other was found at triple junctions. The regions of secondary phases were too

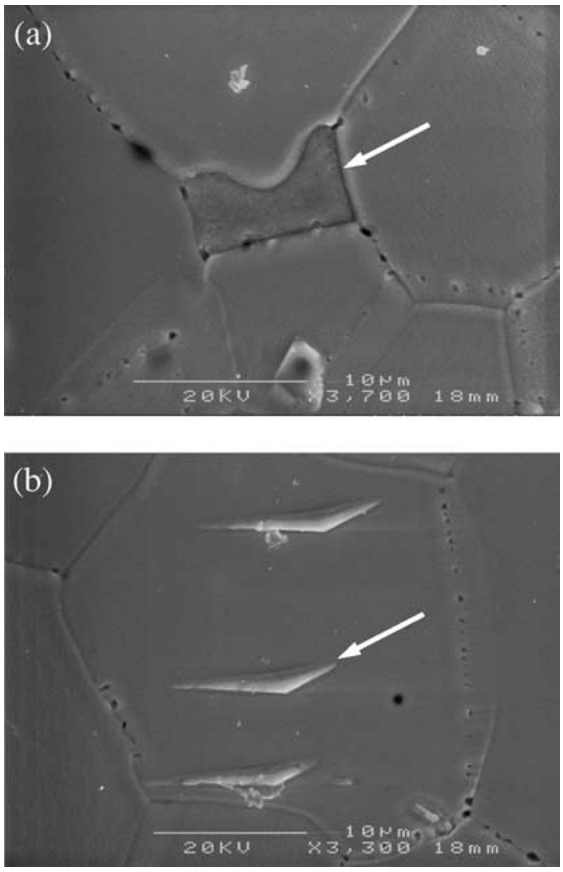

Fig. 6. SEM micrographs of polished, thermally-etched surfaces of LSGM ceramics showing (a) $LaSrGa_3O_7$ and (b) $LaSrGaO_4$ secondary phases.

small to perform quantitative energy dispersive spectroscopy. Comparison of the SEM images with those obtained in another study [6] indicated that the phase at the triple junctions was $LaSrGa_3O_7$ and the plate-like phase was $LaSrGaO_4$. $LaSrGa_3O_7$ and $LaSrGaO_4$ secondary phases are shown in Fig. 6(a) and (b), respectively. The grain size of the ceramics was in the range 5 to 30 μm. Ceramic densities were approximately 95% of the theoretical X-ray density.

A typical Z^* plot of a LSGM ceramic measured at 232°C is shown in Fig. 4 and consists of a single depressed arc with a low frequency 'spike'. The capacitance of the spike, calculated at several frequencies using the relationship $C = 1/\omega|Z''|$ was approximately 0.1 μF, typical of an electrode response for an oxide-ion conductor with partially-blocking gold electrodes. The arc and spike were therefore assumed to be the response of the ceramic and the electrode/sample interface, respectively. For the same data set measured at 232°C, used in Fig. 4, log-log spectroscopic plots of the real and imaginary components of all four formalisms are shown in Fig. 7. Salient features include:

(i) a peak in Z'' and M'' plots, with $f_{max} \sim 50$ kHz (Fig. 7(a)), and ~100 kHz (Fig. 7(b)), respectively. The gradients of the low and high frequency arms of the Z'' and M'' plots, respectively, deviate from the values of 1 and −1 expected for ideal Debye behaviour [7],
(ii) a low frequency plateau at <5 kHz and a high frequency dispersion at >100 kHz in the Y' plot (Fig. 7(c)),
(iii) two overlapping plateau regions, arrowed, centred at 10 kHz and 5 MHz in the ε' plot (Fig. 7(d)), and
(iv) a low frequency electrode response at <1 kHz seen most clearly in Z'', M', Y'' and ε' plots.

Z^* plots of the data measured at 190°C (open symbols) and the best-fit simulations (crosses) for circuits *A*–*D* are shown in Fig. 8(a)–(d), respectively. For circuit *A*, a very poor fit is observed since the measured data exhibit marked non-ideal Debye-like behaviour. In contrast, circuits *B*–*D*, which contain CPEs to model non-ideal behaviour, give much better fits. For circuit *B*, small deviations are observed at most frequencies; *C* and *D* appear to fit the data with reasonable accuracy. Only circuits *C* and *D* are considered for a more detailed analysis.

log-log spectroscopic plots of the real and imaginary parts of each formalism for the measured and best-fit simulated data for circuits *C* and *D* are shown in Figs. 9 and 10, respectively.

Circuit *C* gives a good fit to the peak in the Z'' spectroscopic plot, Fig. 9(a), but over-estimates the M'' data at high frequencies (Fig. 9(b)). The fit to the Y' data also deviates above 10^5 Hz (Fig. 9(c)). Conversely, the fit to the ε' data deviates below ~1 kHz (Fig. 9(d)).

Circuit *D* gives the best fit to all the data at 190°C: all features are modelled satisfactorily over the entire fitted frequency range (Fig. 10). The final fitted values for the 190°C data were $R_{D1} = 3.5\ M\Omega$, $R_{D2} = 0.97\ M\Omega$, $C_{D1} = 3.0$ pF, $C_{D2} = 37$ pF and $n = 0.59$ (fixed at 182°C value) and $\mathrm{A} = 3.3 \times 10^{-10}$ S s^n for CPE_D.

Circuit *D* also gave the best fit for the other data sets in the temperature range (not shown). Arrhenius plots of R_{D1}^{-1} and R_{D2}^{-1} from fits of circuit *D*, are shown in Fig. 11 and both have activation energies of ~1.0 ± 0.05 eV. C_{D1} and C_{D2} were within

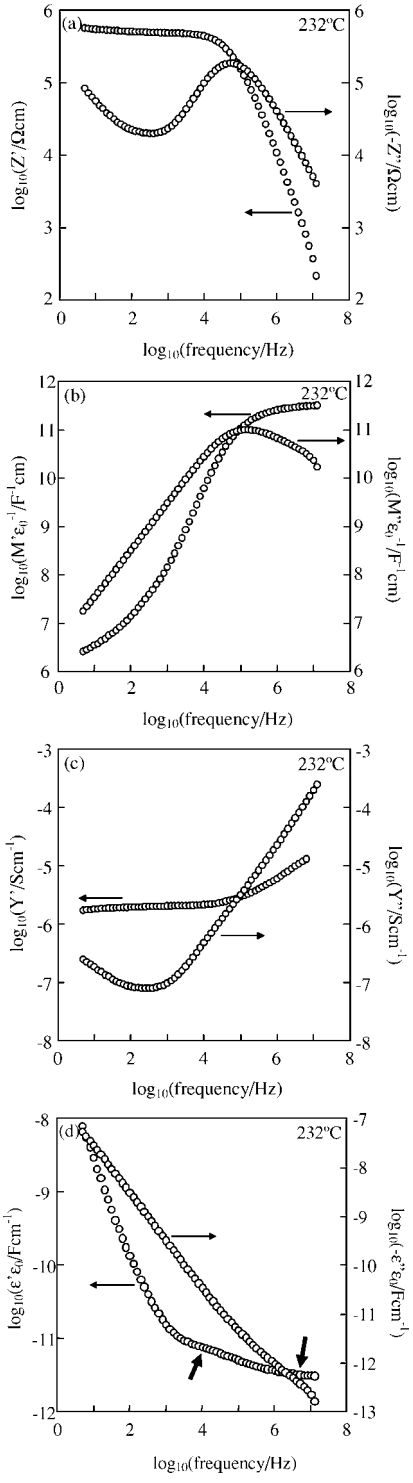

Fig. 7. log-log spectroscopic plots of the real and imaginary parts of Z^* (a), M^* (b), Y^* (c) and ε^* (d) measured at 232°C. ε' plateau regions are indicated by short arrows.

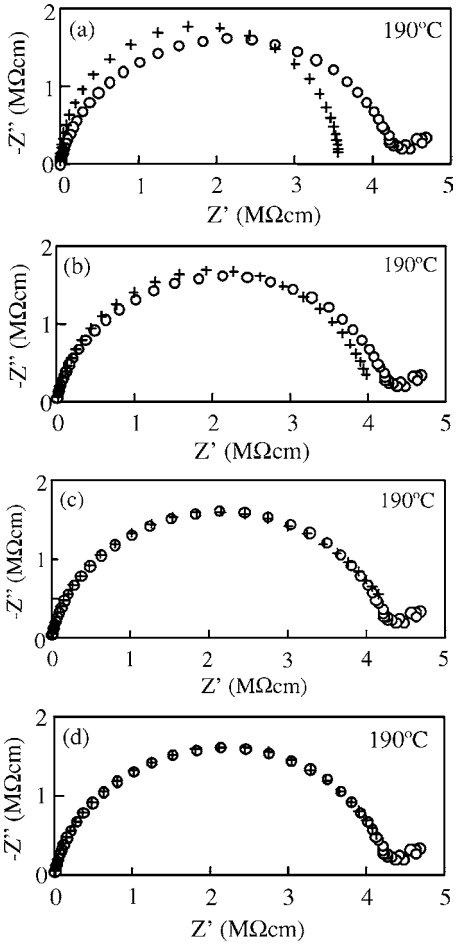

Fig. 8. Z^* plots of data measured at 190°C (open symbols) and the best-fit simulations (crosses) for circuits *A* (a), *B* (b), *C* (c) and *D* (d).

the range 3.0 to 3.2 pF and 33 to 38 pF, respectively. A for CPE_D increased with temperature from 2.8×10^{-10} to 16×10^{-10} S s^n. Plots of $\ln(R_{D1}^{-1}T)$ and $\ln[A\cos(n\pi/2)\,T]$ against reciprocal temperature using the fitted values for circuit *D* are linear with associated activation energies of 1.1 eV and 0.44 eV, respectively, as shown in Fig. 12.

5. Discussion

Circuit *D* gives the best fit to the data in all four formalisms over the measured temperature range. The magnitude of C_{D1}, ~3 pF, is a typical bulk capacitance and an n value of 0.59 and A value of $\sim 10^{-10}$ S s^n for

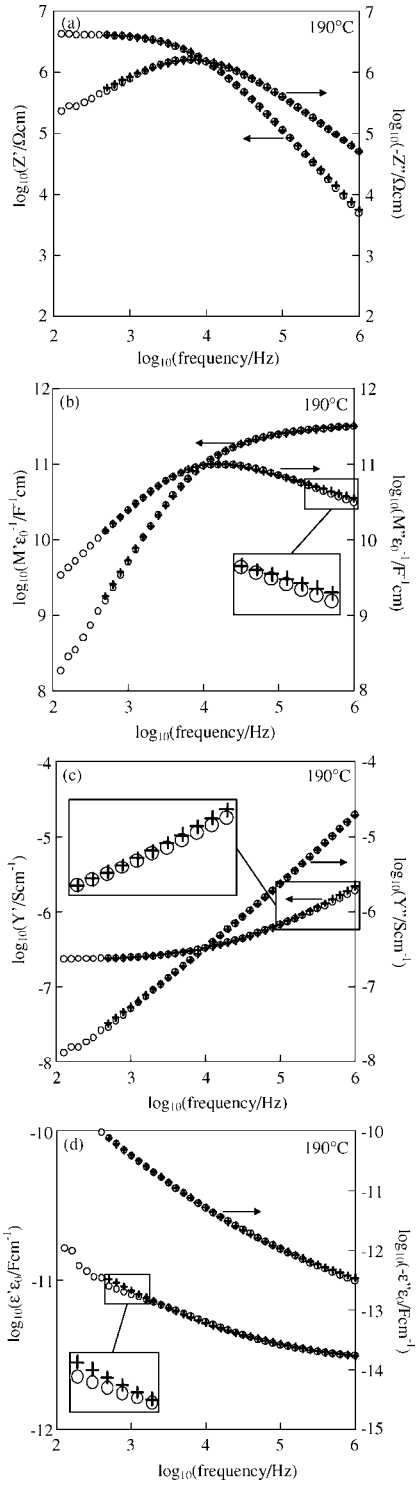

Fig. 9. log-log spectroscopic plots of the real and imaginary parts of Z^* (a), M^* (b), Y^* (c) and ε^* (d) measured at 190°C (open symbols) and the best-fit simulation (crosses) for circuit *C*.

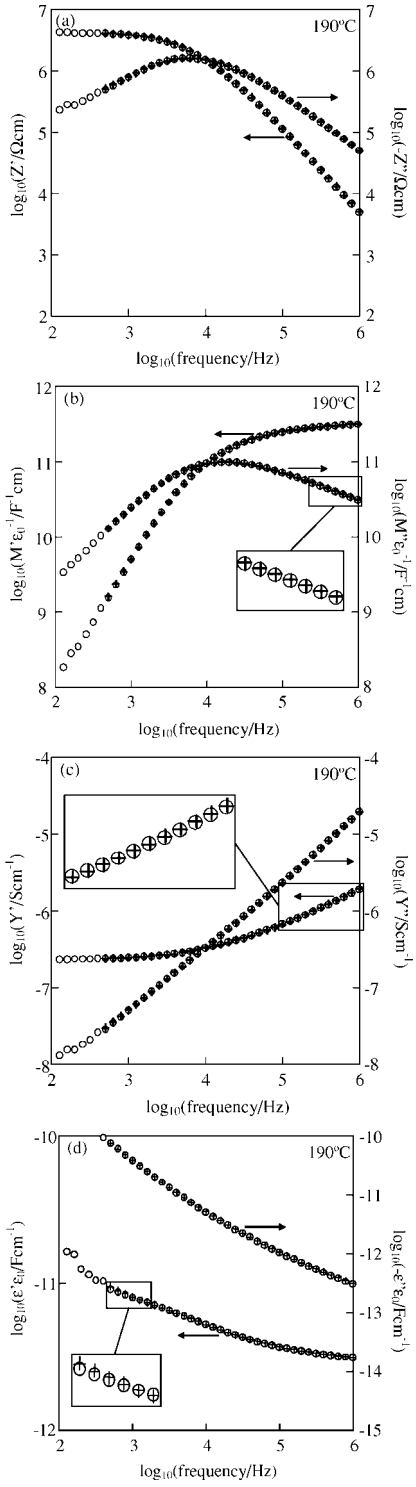

Fig. 10. log-log spectroscopic plots of the real and imaginary parts of Z^* (a), M^* (b), Y^* (c) and ε^* (d) measured at 190°C (open symbols) and the best-fit simulation (crosses) for circuit *D*.

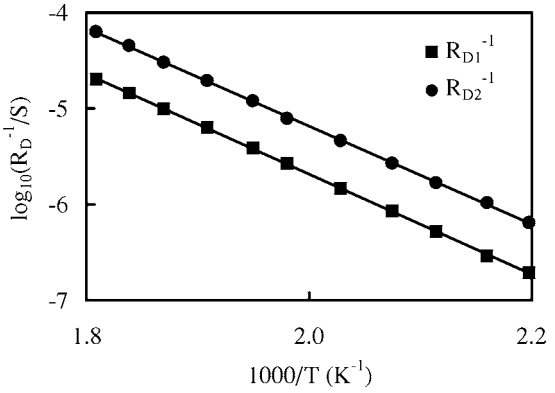

Fig. 11. Arrhenius plot of fitted values of R_{D1}^{-1} and R_{D2}^{-1} from circuit *D* for the temperature range 182 to 280°C.

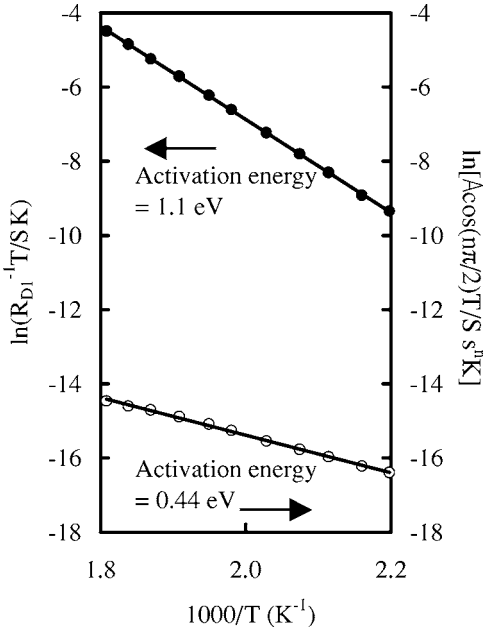

Fig. 12. Plots of $\ln(R_{D1}^{-1}T)$ and $\ln[\mathrm{A}\ \cos(n\pi/2)T]$ against reciprocal temperature using fitted values for circuit *D* for the temperature range 182 to 280°C.

CPE_D are typical for a good ionic conductor [8]. The parallel combination of R_{D1}, C_{D1} and CPE_D in circuit *D* therefore represents the bulk component of the LSGM ceramics. The Arrhenius plot of R_{D1}^{-1} gives an activation energy of ~1.0 eV which compares well with the value of 1.08 eV reported for $La_{0.8}Sr_{0.2}Ga_{0.83}Mg_{0.17}O_{2.815}$ by Huang et al. [9].

The gradient of $\ln[\mathrm{A}\cos(n\pi/2)T]$ against reciprocal temperature is approximately equal to the gradient of $\ln(R_{D1}^{-1}T)$ against reciprocal temperature multiplied by $(1-n)$ (Fig. 12), in agreement with predictions by Almond and West [2] for ionic conductors with temperature independent carrier concentrations.

The magnitude of C_{D2} and the similar activation energies for R_{D1} and R_{D2} suggest that the parallel combination of R_{D2} and C_{D2} represents a constriction resistance within the ceramic, as opposed to a grain boundary response associated with a secondary phase. C_{D2} is approximately one order of magnitude larger than C_{D1} and therefore, the feature giving rise to the current constriction is expected to be approximately ten times smaller than the grain size. Possible origins of the current constriction include the presence of the intragranular, plate-like $LaSrGaO_4$ (electrically insulating) secondary phase and/or pores at the grain boundaries, Fig. 6. Since sputtered gold electrodes were used, constriction resistances due to poor electrode-ceramic contact [10] were unlikely. Further work is required to establish the source of the constriction resistance.

The results shown in Figs. 9 and 10 illustrate the value of using log-log spectroscopic plots of all four formalisms to critically assess fitted data and establish the most probable equivalent circuit. They also illustrate the value of making visual estimates of fitting quality rather than relying on error bars associated with computer-fitting procedures. The different formalisms highlight different aspects of the same data and therefore, close examination of all real and imaginary parts over a wide frequency range helps discriminate between circuits which at first sight give 'good' fits to Z^* plots on linear scales. Thus, although circuits *C* and *D* both fit the Z^* plots, only circuit *D* can model the overlapping plateau regions in the ε' spectroscopic plots. This is because the Z^* plots are dominated by the larger resistance associated with the bulk response (R_{D1}) and it is difficult to detect the presence of a second, smaller arc at low frequencies associated with the constriction resistance (R_{D2}), especially as R_{D1} and R_{D2} have the same activation energy. In contrast, the intermediate frequency data in the ε' spectroscopic plots are dominated by the larger capacitance (C_{D2}) associated with the constriction resistance. The presence of the (poorly resolved) intermediate frequency plateau in the ε' spectroscopic plots therefore highlights the need for an additional parallel *RC* element in series with the element that models the bulk response.

For the data sets analysed here, we have deliberately chosen a temperature range that gave adequate

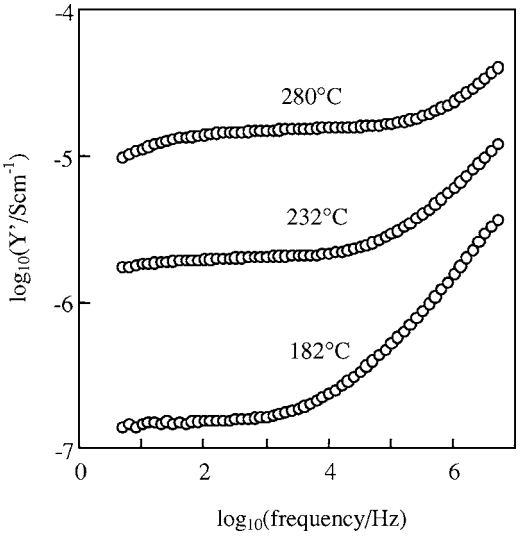

Fig. 13. log-log Y' spectroscopic plots of data measured at 182, 232 and 280°C.

access, at low temperatures, to the bulk response. Let us consider now the consequences of not having such information available to guide the analysis of higher temperature data. It is certainly possible to obtain a good fit to high temperature data using an incorrect circuit such as circuit *B* or *C*, by allowing *n* to vary with temperature. Thus, at 280°C, where there is very little information associated with the high frequency dispersion in Y' compared to lower temperatures (Fig. 13), the fits of circuits *B* and *C* to the data are excellent, as shown for circuit *B* in a Z^* plot (Fig. 14). In the absence of adequate bulk data, therefore, it is not possible to distinguish circuits *B*, *C* and *D*. The values of R_B and R_C that are obtained are both approximately equal to the total resistance of the ceramic at 280°C, as would be expected. The only indication that these circuits are

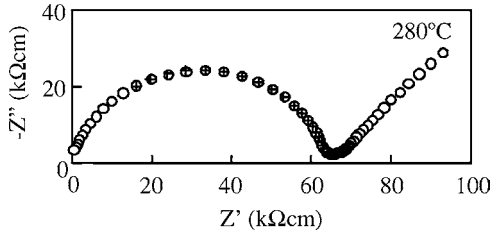

Fig. 14. Z^* plot of data measured at 280°C (open symbols) and the best-fit simulation (crosses) for circuit *B* with the *n* value for CPE_B allowed to refine.

not suitable models, is that the value of C_C, 0.5(2) pF, is too low to be associated with a typical bulk response; there is no indication from the quality of the fits at high temperatures that the sample impedance contains a significant grain boundary contribution and therefore, that the extracted values of R_B and R_C provide an overestimate of the true bulk resistance.

The value of obtaining impedance data over a temperature range, and scrutinising the temperature dependence of the extracted *R* and *C* values, is shown by the consequences of selecting completely inappropriate input values of R_{D1} and R_{D2} in fitting data using circuit *D*. By using $R_{D2} = 0.025R_{D1}$ as input values (instead of $R_{D2} = 0.25R_{D1}$ as used for the refinements above), satisfactory refinement in a (false) minimum was obtained, by either fixing *n* at the 182°C refined value or allowing it to vary for each temperature. Results from fitting the data using circuit *D* with the conditions:

(1) *n* fixed at 182°C value and $R_{D2} = 0.25\ R_{D1}$ inputted,
(2) *n* refined (variable) for each temperature and $R_{D2} = 0.25\ R_{D1}$ inputted,
(3) *n* fixed at 182°C value and $R_{D2} = 0.025\ R_{D1}$ inputted, and
(4) *n* refined for each temperature and $R_{D2} = 0.025R_{D1}$ inputted,

are shown in Figs. 15 and 16.

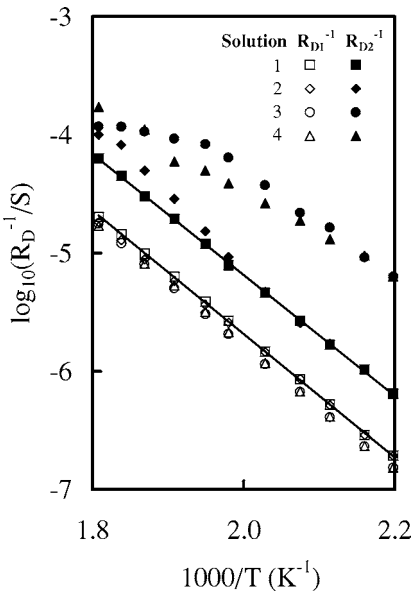

Fig. 15. Arrhenius plots of R_{D1}^{-1} and R_{D2}^{-1} from solutions 1, 2, 3 and 4 for circuit *D*.

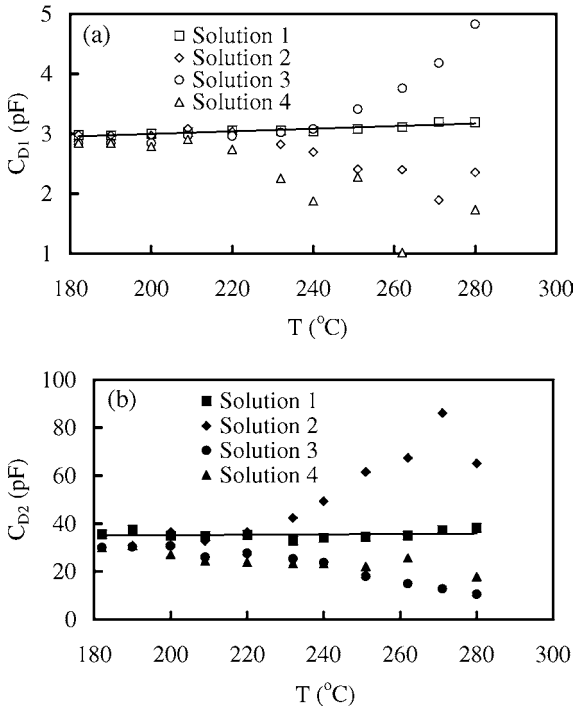

Fig. 16. Variation with temperature of C_{D1} and C_{D2} for solutions 1, 2, 3 and 4 for circuit *D*.

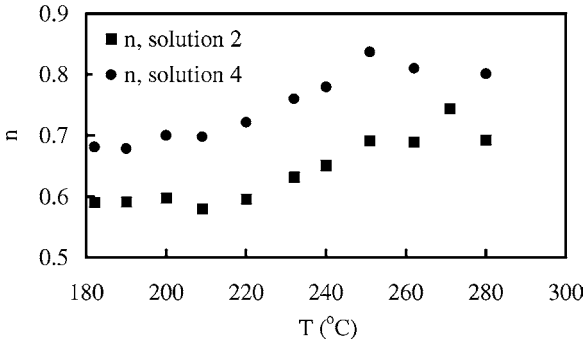

Fig. 17. Variation with temperature of *n* for CPE_D from solutions 2 and 4 for circuit *D*.

It is quite clear from the temperature dependence of the *R* and *C* parameters that only solution 1 is valid. Solution 1 gives linear R_{D1}^{-1} and R_{D2}^{-1} Arrhenius plots and approximately temperature independent C_{D1} and C_{D2} values. There are, of course, many well-established cases where non-linear Arrhenius plots do occur, such as around extrinsic-intrinsic crossover regions or associated with various kinds of phase transitions [11]. Our point is that linear Arrhenius plots provide good evidence that data analysis has been carried out satisfactorily whereas caution is needed over the interpretation of non-linear Arrhenius plots since these could arise from incorrect data analysis.

The variation of *n* with temperature for solutions 2 and 4 is shown in Fig. 17. *n* varied little at lower temperatures where there are adequate data pertaining to the dispersion in Y' spectroscopic plots. At temperatures above 220°C, however, *n* gradually increased with increasing temperature which is an additional pointer that these solutions are incorrect. The gradual loss of data associated with the bulk response with increasing temperature was simulated by reducing the maximum frequency employed in fitting the data with solution 2 for circuit *D* at 220°C. *n* increased as the maximum frequency cut-off value decreased, Table 1, thus indicating that the increase in *n* when fitting higher temperature data may be an artefact due to the loss of data associated with the dispersion region, rather than to an intrinsic property of LSGM. This analysis, therefore, justifies fixing *n* at the 182°C value during the fitting of higher temperature data.

Although circuit *D* has a larger number of fit parameters compared to the other circuits, it clearly fits the data better when the entire range of temperatures is considered, especially at low temperatures where only circuit *D* gives a good fit. It is possible that some alternative circuit with the same number of fit parameters could, in principle, fit the data equally as well as circuit *D*; however, circuit *D* is related directly to the assumed brickwork model of the ceramic microstructure. Since, within errors, our data are accurately fitted by circuit *D*, which is a one dimensional representation of the brickwork model, and the values of the extracted parameters are reasonable and have a sensible temperature dependence, we regard this as a valid

Table 1. The variation of the fitted value of *n* as a function of the maximum frequency cut-off value for solution 2

Maximum frequency cut-off (Hz)	*n*
1.0×10^6	0.60
6.3×10^5	0.61
4.0×10^5	0.62
2.5×10^5	0.64
1.6×10^5	0.65
1.0×10^5	0.68
6.3×10^4	0.71

working model with which to analyse the impedance data. It may be that, in practice, a two or three dimensional model provides a more accurate description of the impedance response, as discussed by Fleig and Maier [12–14], but there is no experimental justification for the use of such a more complex model in this case.

6. Conclusions

The electrical behaviour of oxide-ion conducting $La_{0.80}Sr_{0.20}Ga_{0.83}Mg_{0.17}O_{2.82}$ ceramics was modelled successfully using an equivalent electrical circuit consisting of a parallel combination of a resistor, capacitor and CPE to model the bulk response, connected in series with a parallel combination of a resistor and capacitor to model the response of a constriction resistance. To identify and deconvolute these two responses it was necessary to analyse IS data using log-log spectroscopic plots of the real and imaginary parts of all four complex formalisms over a temperature range between 182 and 280°C. Alternative equivalent circuits were eliminated by critically assessing the quality of fit to the measured data over a range of frequency and temperature.

It is probably true to say that the reasons why impedance data often show departures from Debye-like ideality are not well-understood. At the simplest level, n and A may be regarded as adjustable fitting parameters. Nevertheless, n and A are parameters whose temperature (in)dependence is usually well-behaved and their satisfactory inclusion in data analysis helps greatly in discriminating between competing model circuits.

Acknowledgments

We thank the EPSRC for funding.

References

1. J.T.S. Irvine, D.C. Sinclair, and A.R. West, *Advanced Materials*, **2**, 132 (1990).
2. D.P. Almond and A.R. West, *Solid State Ionics*, **9/10**, 277 (1983).
3. D.C. Sinclair and A.R. West, *Journal of Applied Physics*, **66**(8), 3850 (1989).
4. A.K. Jonscher, *Nature*, **267**, 673 (1977).
5. ZView Version 2.1b, Derek Johnson, Scribner Associates, Inc.
6. K. Huang, R.S. Tichy, and J.B. Goodenough, *Journal of the American Ceramic Society*, **81**(10), 2576 (1998).
7. A.R. West, D.C. Sinclair, and N. Hirose, *Journal of Electroceramics*, **1**(1), 65 (1997).
8. R.J. Grant, I.M. Hodge, M.D. Ingram, and A.R. West, *Nature*, **266**(5597), 42 (1977).
9. K. Huang, R.S. Tichy, and J.B. Goodenough, *Journal of the American Ceramic Society*, **81**(10), 2565 (1998).
10. E.J. Abram, D.C. Sinclair, and A.R. West, *Journal of Electroceramics*, **7**, 179 (2001).
11. D.C. Sinclair and A.R. West, *Physical Review B*, **39**, 13486 (1989).
12. J. Fleig and J. Maier, *Journal of the Electrochemical Society*, **145**(6), 2081 (1998).
13. J. Fleig and J. Maier, *Journal of the European Ceramic Society*, **19**, 693 (1999).
14. J. Fleig and J. Maier, *Journal of the American Ceramic Society*, **82**(12), 3485 (1999).